Supplemental Information

Table S1: Comparative overview of state-of-the-art oxygen and pH sensing platforms

|		MICROENVIRONMENT	THROUGHPUT	SENSORS AND SENSING PRINCIPLE	ADDITIONAL COMMENTS
COMMERCIALIZED	MitoXpress assay (Agilent)	Static	High	Dispersed Oxygen and pH Probes	Requires mineral oil → potential extraction of lipophilic substances; Assay time: 60-90 min
	Seahorse XF analyzer platform (Agilent)	Static	High	Optical O_2 and pH measurement	Up to 4 compounds can be added; Assay time: 60-90 min
	O2k-FluoRespirometer (Orobos)	Static	Low	Electrochemical O_2 and pH measurement	Invasive Requires Permeabilized Tissues or Cells, Individual Cells
	SC 1000 Metabolic Chip (Bionas)	Dynamic	Low N=6 Big Footprint	Electrochemical O_2 and pH measurement	Non-invasive monitoring; Limited Optical Access; Discontinued
	Biochip D (Cellasys) IMOLA-IVD	Dynamic	Low N=6 Big Footprint	Electrochemical O_2 and pH measurement	Non-invasive monitoring; Optical Access
ACADEMIC	Tanumihardja et al.[40]	Static	Low N=1	Electrochemical O_2 and pH measurement	Sensor integrated Transwell system; Oxygen sensing cannot be performed more than once per hour; ECAR
	Shaegh et al.[41]	Dynamic	Low N=1	Optical O_2 and pH (absorption) measurement	Non-invasive monitoring; Design limitation due to absorption-based detection approach
	Lee et al.[42]	Dynamic	Low N=1	Optical O_2 and pH measurement	Microfluidic continuous culture reactors with high working volumes of 1 mL for bacterial cultures; Non-invasive monitoring
	Weltin et al.[43]	Dynamic	Low N=1	Electrochemical O_2 and pH measurement	Proof of Principle; Non-invasive monitoring of T98G human brain cancer cells
	Huang et al.[44]	Dynamic	Low N=1	Optical O_2 and pH measurement	Monitoring of OCR and ECAR of a developing zebrafish; Non-invasive monitoring; No optical access in sensor integrated setup
	Dual sensor-integrated prototype	Dynamic	Moderate N=8 (36x76 cm)	Optical O_2 and pH measurement	Low Footprint; Non-invasive monitoring; Cellular Viability < 60 s
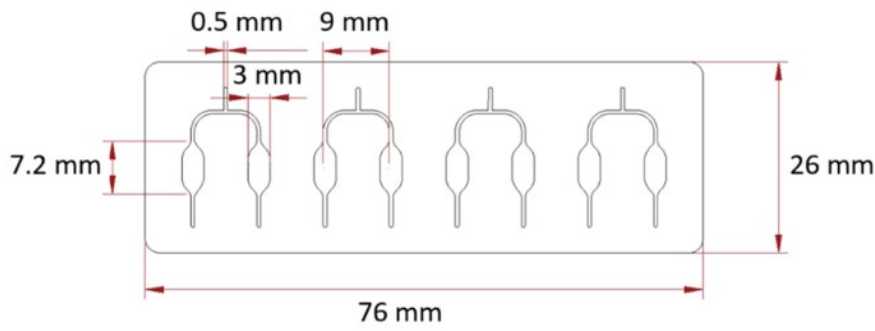
Figure SI1: Schematic illustration of the COC microfluidic prototype with the individual dimensions of the chip, the chambers, and the microfluidic channels.
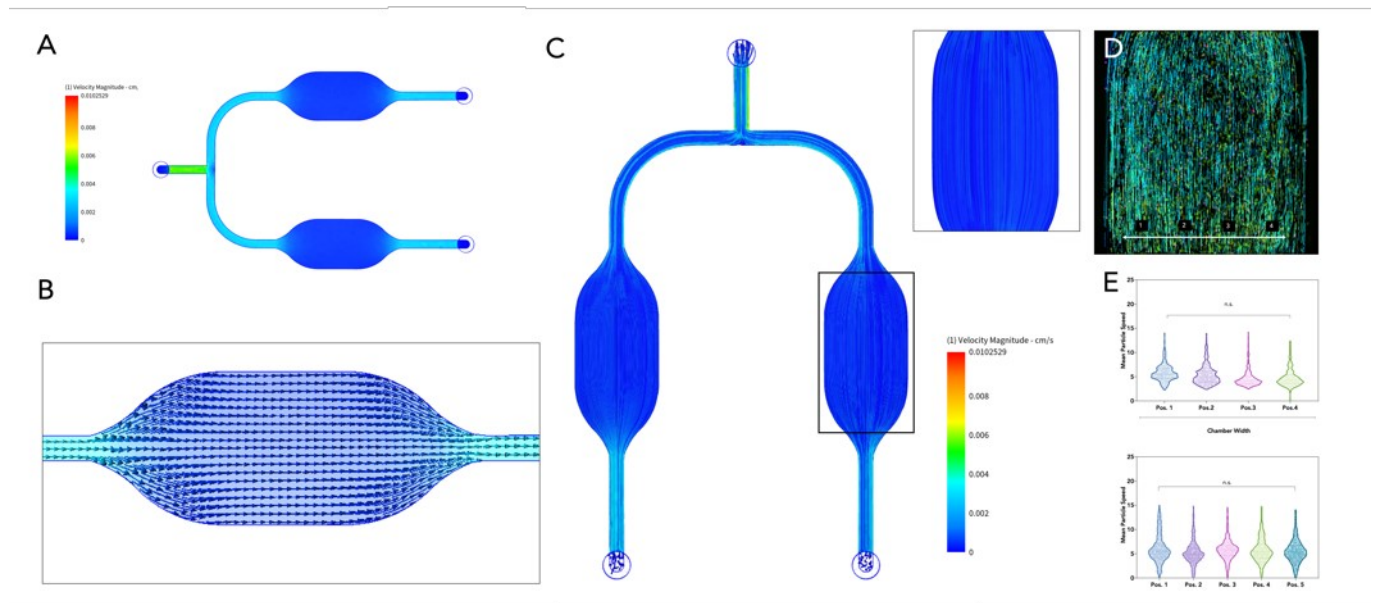

Figure SI2: CFD analysis of the microfluidic prototype. a) Simulated flow behavior through the cell culture chambers (h:280 µm) at a flow rate of 10 µL/min, depicting a uniform flow profile with parallelly aligned streamlines. b) Simulated particle distribution within the microfluidic chamber at a flow rate of 10 µL/min. c) Representative image of the tracked particles within the microfluidic chamber. d) Comparative analysis of the mean particle speed along the width of the microfluidic chamber and at five randomly located positions within the device, revealing no significant difference and thus a uniform particle distribution through the chamber.
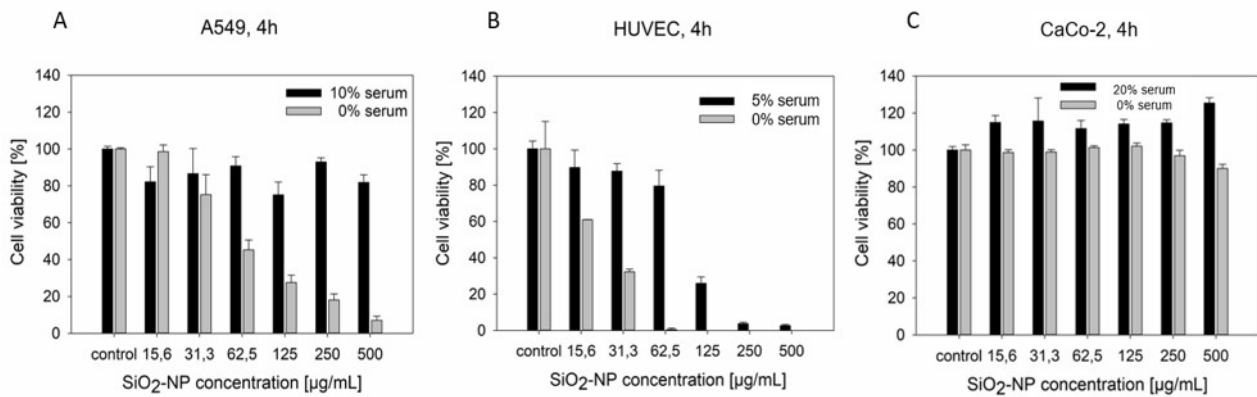
Figure SI3: Cell viability of (a) A549 cells, (b) HUVECs, and (c) Caco-2 cells in standard 48-well plates after 4h SiO$_2$-NP exposure of increasing concentrations in medium with and without serum determined with a Presto Blue assay. The signals of untreated cells were set as 100%. The plotted data represent the mean ± standard deviation (CV: %), n = 3.
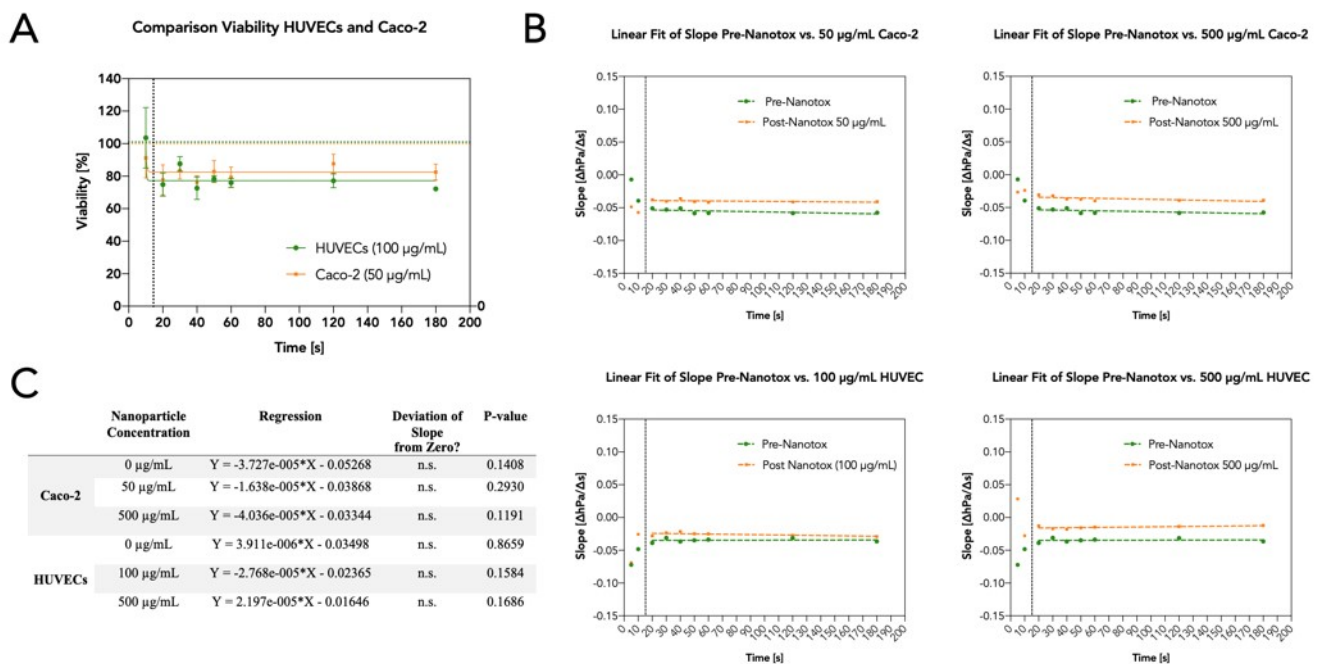

	Nanoparticle Concentration	Regression	Deviation of Slope from Zero?	P-value
Caco-2	0 µg/mL	Y = -3.727e-005*X - 0.05268	n.s.	0.1408
	50 µg/mL	Y = -1.638e-005*X - 0.03868	n.s.	0.2930
	500 µg/mL	Y = -4.036e-005*X - 0.03344	n.s.	0.1191
HUVECs	0 µg/mL	Y = 3.911e-006*X - 0.03498	n.s.	0.8659
	100 µg/mL	Y = -2.768e-005*X - 0.02365	n.s.	0.1584
	500 µg/mL	Y = 2.197e-005*X - 0.01646	n.s.	0.1686

Figure SI4: Assay time validation. a) Viability calculations for HUVECs (green (CoV < 5%)) and Caco-2 (orange (CoV < 7%)) for three individual experiments at different measurement time points (10s-180s) revealing comparable viability results after 20 seconds of measurement. b) Comparative analysis of the acquired slopes (ΔhPa/Δs) for HUVECs and Caco-2 cells prior (green) and after (orange) different nanoparticle exposure scenarios revealing stable slopes after 20 seconds of measurement. Slopes were fitted with a linear regression. c) Table listing the linear regression equations and the deviation of the respective slopes from 0.
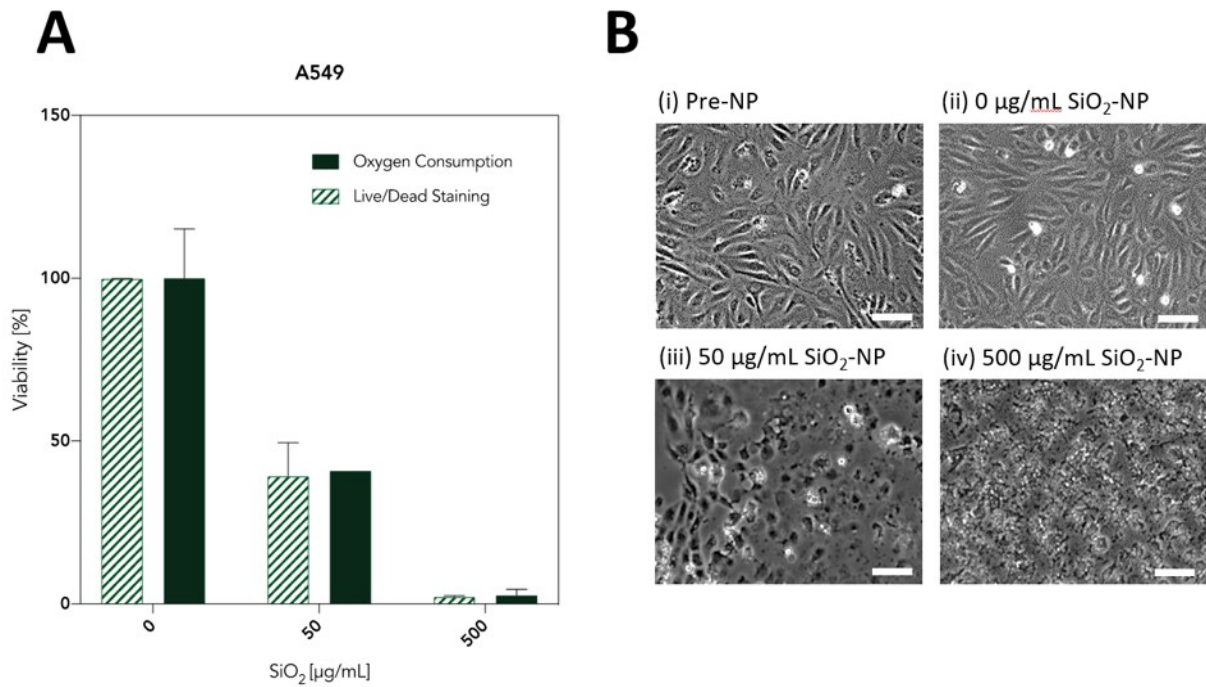
Figure SI5: Effect of SiO$_2$-NP on cell viability and cell morphology in A549 cells after 3h perfusion in microfluidic cell culture chambers with the glass prototype. (A) Cell viability calculated from oxygen consumption and from Live/Dead staining both showed dose-dependent decreases at comparable rates. The plotted data represent the mean ± standard deviation (CV: 1.5-15.6 %), *n* = 3. (B) Morphology studies of A549 cells (i) after over-night proliferation in standard culture medium showed a typical cobblestone morphology with triangular shapes. (ii) After 3 h perfusion of serum-free medium (control) about 50% of the cells have contained their triangular shape while the rest transformed into rounded shapes. (iii) After exposure with 50 μg/mL SiO$_2$-NP the majority (>90%) of cells had lost cell-cell contacts and changed the morphology into rounded shapes, probably caused by a combination of nanoparticle exposure and the serum-free medium. Despite this, the cells did not detach from the substrate during flow conditions. (iv) After exposure with 500 μg/mL, the cells showed both rounded shapes as well as fragmentized morphology typical of dead cells. Scale bar: 100 μm. 10x magnification.
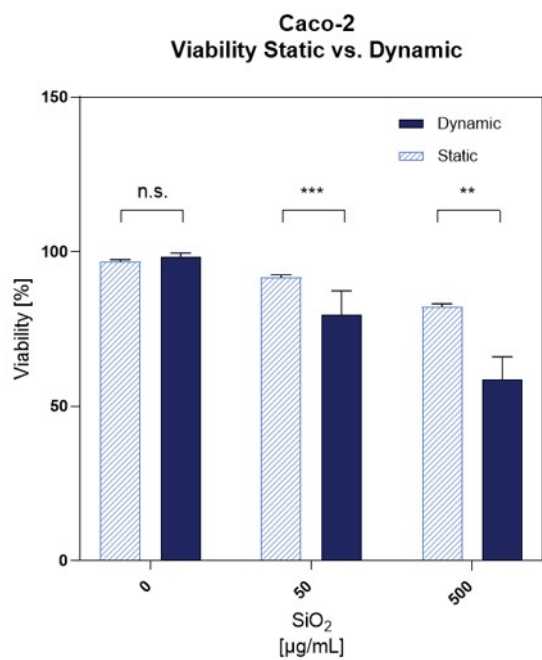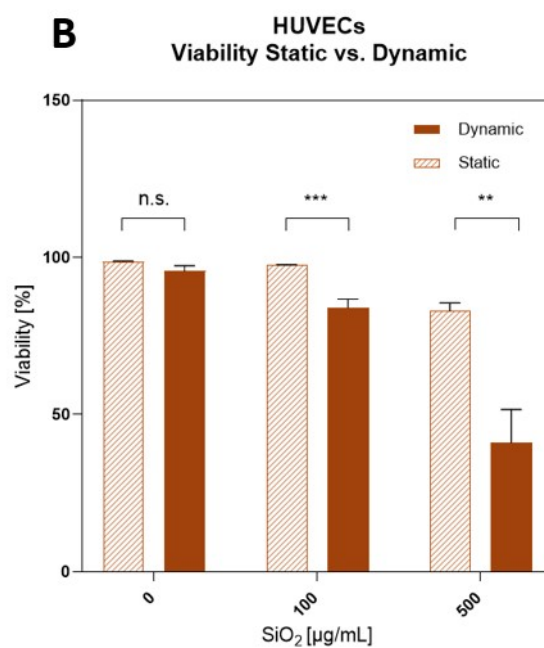
Figure SI6: Impact of static and dynamic silica nanoparticles exposure scenarios on (a) Caco-2 cells (20% FCS) and (b) HUVECs (serum free). The plotted are derived from the live/dead assays and expressed as mean value ± SD (n= 3-9).